Comparison of Laser and Differential GPS Ranging Approaches

Walton Williamson,* Keith Wilson,† Joseph Kovalik,†
Malcolm Wright,† Bruce Haines,* and Yoaz Bar-Sever*

As part of a larger effort to validate Global Positioning System (GPS) techniques for global centimeter-level positioning of aircraft using laser ranging, this article reports on a dynamic ground experiment that uses an optical laser ranging system to validate the accuracy of differential carrier phase GPS. The laser is located at the Jet Propulsion Laboratory Optical Communications Telescope Laboratory, Table Mountain, California, and transmitted a 100-Mb/s pseudorandom noise data stream that was retroreflected from a moving truck on an adjacent mountain peak. GPS measurements were collected from two survey-grade commercial receivers: one antenna was located near the laser and the second on the truck. The GPS measurements are processed using a short-baseline, wide-lane, differential carrier phase solution to estimate the relative position of the ground vehicle relative to the static base station. The laser ranging results are compared with the GPS solution. Results show agreement to an average of 4.2 cm (RMS) between the laser and the differential GPS over four different runs.

I. Introduction

This article reports on a ground-based experiment to validate a new laser ranging device and a Global Positioning System (GPS) relative position estimation scheme. Both the laser and the software for processing the GPS data were developed at the Jet Propulsion Laboratory (JPL). The goal of these tests was to compare the laser and differential GPS range solutions and to determine the challenges to achieving agreement to within 10 cm root-mean-square (RMS) during dynamic tests. For this test, a truck was used as the dynamic target. Future tests will use an aircraft.

The tests took place in Wrightwood, California, at the JPL Table Mountain Facility. The laser and a GPS receiver were placed at the Optical Communications Telescope Laboratory (OCTL) at Table Mountain. A retroreflector and GPS receiver were mounted in the bed of a pick-up truck. The test plan called for the truck to drive up a ski run in the valley below at speeds from 2 to 11 m/s as allowed by the terrain at a distance of 1.2 to 1.5 km from the OCTL. GPS data were collected from both locations and postprocessed. The GPS receivers at

---

both locations were commercial off-the-shelf (COTS) geodetic-quality receivers with choke-ring antennas to mitigate multipath effects. The results showed agreement to an average of 4.2 cm (RMS), meeting the goals of the test.

This article first discusses the short-baseline, differential carrier phase GPS algorithm utilized to process the GPS data, originally developed in [1]. Then the laser, its modulation format, and optical ranging signal-processing techniques are described. Finally, the test setup and test results are presented.

II. Short-Baseline Estimation

GPS code and carrier phase measurements were collected from both the truck and the OCTL ground station in order to form an estimate of the relative position between the two positions. A kinematic differential carrier phase algorithm was implemented to estimate the relative position using carrier phase measurements. Since the GPS receivers utilized can track carrier phase to less than 1 cm, relative positions may be estimated to centimeters. The challenge to achieving accurate centimeter-level range measurements between two locations is resolving the unknown integer ambiguity between the two GPS receivers.

The simplest method for short-baseline processing is to implement a "geometry-free" estimator of the wide-lane carrier phase ambiguity such as the method used to initialize the algorithm presented in [2]. Using this algorithm, the "wide-lane" combination of the L1 and L2 carrier phase measurements from both the truck and the ground station are collected. The wide-lane carrier phase is used to form a double-difference residual and then differenced with the double-differenced "narrow-lane" code combination. This residual, when averaged over time, should provide an estimate of the wide-lane integer ambiguity (assuming no multipath effects). The ambiguity is resolved through statistical testing of the average of the RMS error in the double-differenced residual using assumed noise covariance for code and carrier phase. Once the ambiguity is resolved, the double-differenced carrier phase measurements can be converted to a relative range measurement between the truck and OCTL. These range measurements are processed through a least-squares estimation technique to determine the relative positions of the truck and ground station.

Geometry-free estimates are not sufficient for this application for two reasons. First, the arc lengths are not sufficiently long over the length of the run to properly estimate the integer ambiguity, given assumed measurement noise statistics. Arc lengths were cut short due to satellite blockage. As the truck traveled up the ski run, trees, parts of the ski lift, and the mountain and adjacent mountain peaks obstructed the line of sight to the satellites. Second, reflections from these obstructions posed a significant code multipath problem. An alternative strategy that improved the convergence time of the geometry-free solution was therefore implemented.

The algorithm developed here is similar to that developed in [1] with enhancements for batch-type postprocessing. This algorithm estimates the double-differenced, wide-lane carrier phase integer ambiguity using both code and carrier phase residuals. It is called the

annihilation method because of the manner in which it removes the effects of position uncertainty in the residuals through a linear transformation referred to as an annihilator. The algorithm is combined with a statistical probability test to determine when the integer ambiguity is valid. The method is robust to initial condition errors since it annihilates errors in position estimates in the residuals used for ambiguity detection. It is more robust to multipath because it de-weights the code-based residual by adding a residual using only carrier phase measurements, which is not as susceptible to multipath and has significantly lower noise covariance. It also converges more quickly because it performs a statistical test on the geometry-free residual combined with a carrier-phase-only residual.

The algorithm operates on two sets of double-difference residuals. These residuals are:

(1) The wide-lane carrier minus narrow-lane code residual is the same residual utilized by the geometry-free solution. This residual is equal to the noise in the code and carrier phase measurements plus a bias due to the unknown wide-lane integer ambiguity.

(2) The wide-lane carrier-phase-only range residual is equal to the noise in the carrier phase measurements plus the unknown integer ambiguity. In addition, an a priori estimate of the relative range is required. An annihilator is utilized to remove the error in the relative range estimate, leaving only carrier phase noise and the integer ambiguity. It is not as susceptible to multipath and has lower overall noise statistics compared to the residual using code and carrier phase. Correlations between the residuals are small.

Because the carrier-phase-only residual is affected by the initial condition errors and any errors in the best estimate of the integer ambiguity, we use an annihilator that is designed to remove the errors associated with the relative position uncertainty. The remaining uncertainty is due to the unknown integer ambiguity method. If the correct integer ambiguity is found, both residuals should be zero-mean Gaussian processes since the integer ambiguity is discrete and not a floating parameter. The method used in this experiment invokes a statistical hypothesis testing scheme to help identify the correct integer vector. Each integer combination is hypothesized and the residual that best approximates a zero-mean Gaussian is selected as the most likely integer combination.

The algorithm proceeds with the following basic steps, with details provided in [1].

(1) Record the L1 and L2 carrier phase and code range at both locations.

(2) Calculate satellite orbits and clocks using the GPS broadcast ephemeris.

(3) Estimate the location of each receiver independently using the ionosphere-free code combination, an altitude-based estimate of the troposphere zenith delay, and mapping functions [3]. Estimate the position and clock bias using a least-squares, single-epoch technique.

(4) Utilizing data from both receivers, form the double-differenced, wide-lane carrier phase and the narrow-lane code combination.

(5) Estimate the wide-lane carrier phase integer ambiguity by averaging the difference between the wide-lane carrier phase observable and the narrow-lane code over the available arc length. Estimate one ambiguity for each double-differenced pair. This technique is often referred to as a geometry-free estimation of the wide-lane integer. No knowledge of receiver position is required.

(6) Form a second residual using only the double-differenced, wide-lane carrier phase and the a priori estimate of relative range derived from the least-squares estimate. Neglecting multipath, the only remaining error is in the initial estimate of the least-squares position and the unknown integer ambiguity.

(7) Form an annihilator such that the annihilator multiplied by the carrier range residual removes the effect of the uncertainty in relative position.

(8) Form a combined residual consisting of the annihilated carrier range residual and the geometry-free residual.

(9) Hypothesize a set of wide-lane integers around the geometry-free estimate of the wide-lane integer. Typically ±2 integers for each satellite are sufficient, but more are required if large multipath is experienced.

(10) Add the hypothesized integer to each residual, forming a new residual for every hypothesis combination. The number of hypothesized vectors will be the number of double-differenced residuals to the power of the number of hypotheses per satellite. In order to test ±2 integers on each of five double-differenced residuals (for six satellites in view), a total of 3125 hypotheses is required.

(11) Statistically test each integer combination through a sequential probability ratio test to estimate the probability that each hypothesis is correct given a priori estimates of code and carrier phase. For this experiment, 1-m RMS error was applied for each code measurement and a 1-cm RMS error was applied for each carrier phase measurement.

(12) Select the correct hypothesis when a particular probability reaches a threshold.

(13) Form relative range measurements using the wide-lane carrier phase combined with the hypothesized integer selected by the algorithm. Calculate the relative position using a least-squares estimator on an epoch-by-epoch basis.

(14) If the number of satellites tracked was insufficient at any epoch to generate the required residuals, the relative solution was computed using the ionosphere-free code combination.

This method converges more quickly than geometry-free methods and is immune to errors in the initial condition provided that a sufficient number of hypotheses are chosen to span the uncertainty in the position. In this case, the errors due to code multipath on the initial position estimates are de-weighted by the use of the carrier-phase-only residual. The carrier phase range residuals dominate the statistical test since the carrier phase noise is significantly smaller than the code noise. Because it requires the ability to form double differences, and because it annihilates the effect of position errors, this method requires GPS receivers to track at least five common satellites simultaneously, with six preferred. This is in contrast to a minimal GPS solution that requires only four satellites.

III. Optical Ranging

Laser ranging systems, although commercially available, could not provide the required 10-cm ranging accuracy for the ranges (>5 km) of the planned aircraft experiments. Consequently, JPL developed a laser ranging system that met the range, precision, and eye safety requirements for the Aircraft Laser Uplink Ranging Experiment (ALURE).

Optional approaches for precision optical ranging are direct detection of time of flight of a subnanosecond laser pulse and measuring the time delay by cross-correlating continuous pseudorandom bit streams (PRBS). Safety issues associated with transmission of short, high-power laser pulses made the direct detection an unattractive approach for ranging to a target (a truck or an aircraft) with individuals on board. Opting for the PRBS approach, we developed the laser system shown in Figure 1 specifically for this application.
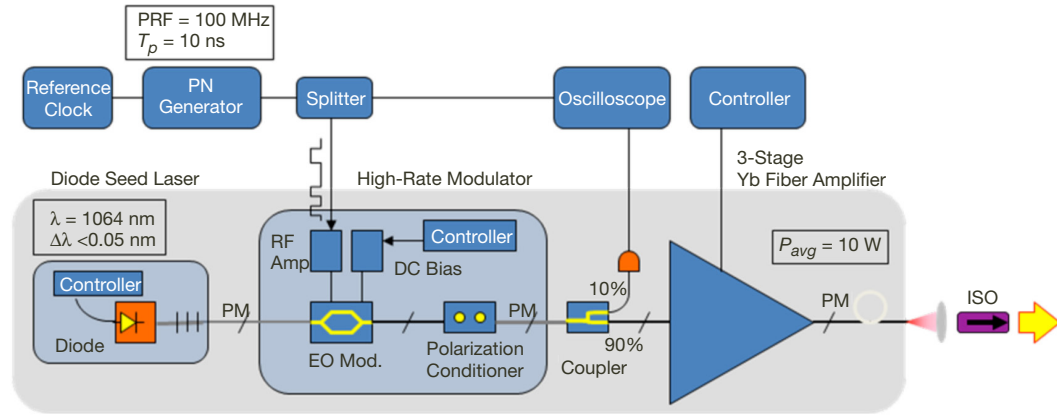

Figure 1. Fiber laser transmitter modulated at 100 Mb/s pseudonoise code.

The laser is a fiber-coupled seed laser modulated at 100 Mb/s followed by a fiber amplifier capable of 10 W average output power. The oscillator is a narrow-linewidth, hybrid external cavity diode laser from Innovative Photonic Solutions (IPS). The output is coupled to a polarization-maintaining (PM) fiber and fed into a 10-GHz electro-optic (EO) modulator driven with a 100-Mb/s PRBS PN 7 data stream. Bias control of the modulator can either be performed manually or through a custom automatic bipolar pulse technique. Automatic bias control was preferred but encountered drift at times, which required manual adjustment. The modulator output is also polarized and coupled into a three-stage 10-W IPG Photonics Yb fiber amplifier. The laser output is limited to a few watts to enable coupling through an isolator to a 10-m-long, optical fiber patch cord used for routing the signal to the telescope assembly on the OCTL roof. To maintain near-single-mode output but allow for high-power coupling at 1064 nm into the fiber patch cord, an SMF28 cable, single-mode at 1550 nm, was used. A portion (10 percent) of the modulator output is monitored on an oscilloscope so the pulse extinction ratio can be optimized through the modulator bias control. For the near-range horizontal tests described herein, the power was limited to approximately 400 mW, although for the future long-range flight experiments, up to 2 W average power output will be possible from the fiber reliably. An optional capability for continued short-range horizontal path calibration experiments included replacing the high-power

IPG amplifier and coupling optics with a two-stage PM 0.4 W Keopsys Yb fiber preamplifier fiber-coupled directly to the patch cord.

The laser output was fiber-coupled to a small collimator at the base of a 20-cm Meade receiver telescope, shown in Figure 2. The $1/e^2$ collimated output beam divergence was 2 mrad. Two mirrors, one at the base of the telescope and another at the rear of the secondary mirror, launched the beam to the target, as seen in Figure 3. Positioning the mirror behind the receiver secondary mirror ensured optimum collection of the return signal by the telescope.
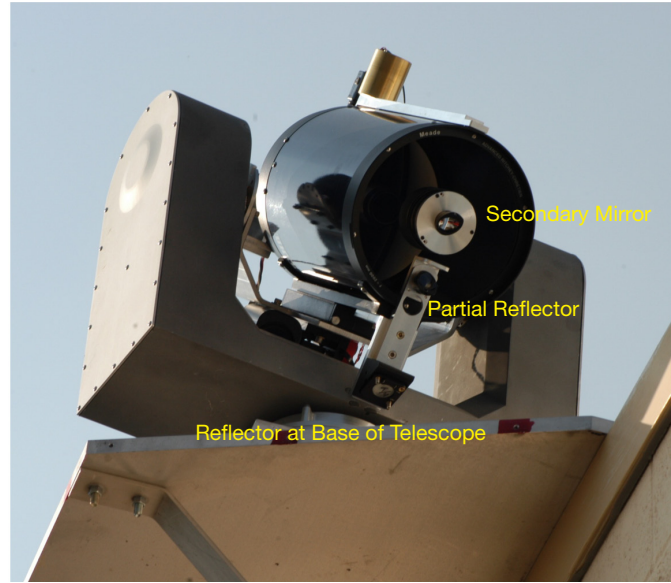

Figure 2. ALURE transceiver, showing laser coupling to Meade telescope.

A 100-μm-thick optical window was positioned and aligned between the two mirrors to reflect a part of the laser beam back into the telescope. This served as a local optical range reference and eliminated range errors due to laser jitter and electronic delays. The range was determined from the difference between the times of the signal reflected from the window and that returned from the target retroreflector. Both the retroreflected and the local optical reference signals were focused onto a 100-MHz bandwidth avalanche photodiode detector (APD). The APD output is coupled to an 8-bit digitizer.

Figure 3 is a schematic of the optical transceiver and data acquisition system. We established the optimum number of samples needed to obtain the desired accuracy. The results of this analysis are given in Figure 4a. The data show that the RMS follows the expected behavior of decreasing as the inverse square root of the sample length. To reduce the contribution of this error source to the range measurement, we used the longest record length possible that would support the required computer processing time for the real-time cross-correlation analysis. In this experiment, a 60-μs (60,000 samples at 1 gigasample/s) record length was used. This was longer than the 32767 (PN15) sequence that was used to cover a maximum distance of 24 km before wrapping ambiguities were introduced.
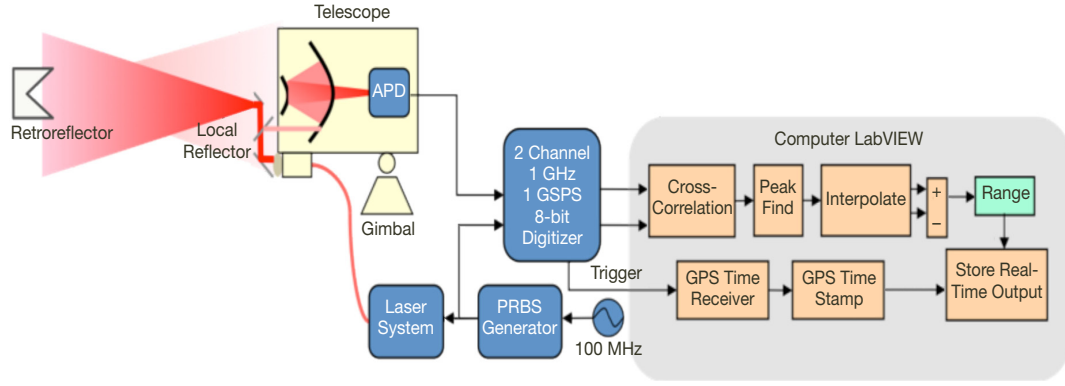
Figure 3. Schematic of optical transceiver.

Although the analysis showed that submillimeter accuracies were achievable with long enough record lengths, the realizable accuracy is determined by the signal-to-noise ratio (SNR) at the detector. The SNR was defined as the ratio of the cross-correlation peak height to the average background cross-correlation signal. Figure 4b plots the standard deviation of the range measurement as a function of the SNR for the actual experimental system used. The standard deviation drops off dramatically initially as the background electronic noise level is overcome. An SNR greater than 4 gives an error of less than 10 cm.

For all the data runs of this experiment, the SNR was between 50–100, which gives 1- to 2-cm-level range error. The detector noise equivalent power (NEP) was 15 nW RMS for the 100-MHz bandwidth used. The results of this analysis guided the selection of retroreflector aperture (15 mm, 25.4 mm, 50 mm) for the different ranges (60 m to >3 km) during the laser transmitter and receiver co-alignment pretests.

The cross-correlation was performed between a reference channel and the returned optical signal. The reference channel is a signal split from the PRBS generator. Since the returned optical signal has both a fixed reference component and a varying one from the actual
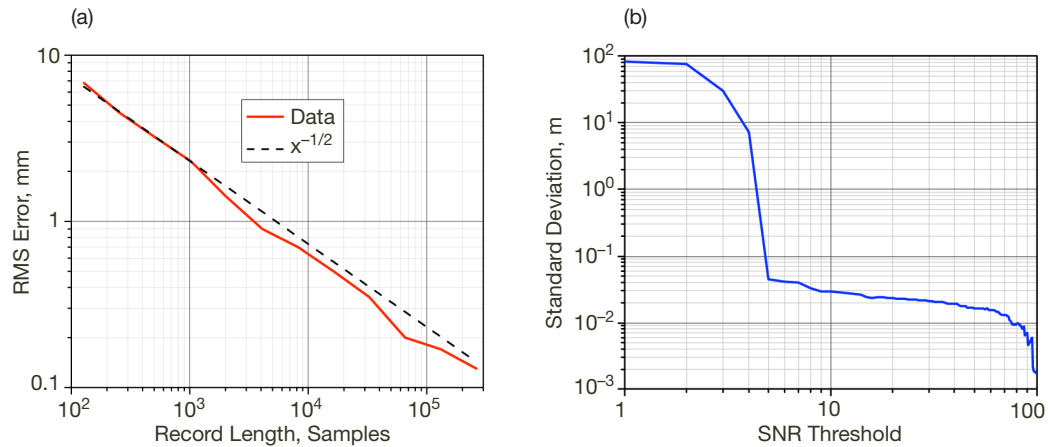

Figure 4. Plots show (a) the reduction in RMS error with record length of data samples, and (b) standard deviation in measurement error as a function of SNR.

range measurement, two cross-correlation peaks are visible. A Labview algorithm was developed to perform the cross-correlation and identify the two correlation peaks in real time. Differencing the time between the near and far peaks eliminated common mode errors due to delays in electronics (~37 m). The data acquisition was timed to occur at the 0.5-s time intervals from a GPS-derived trigger signal. Acquisition (60 μs) and data processing (few hundred μs) would take place in less than the effective 0.5-s sampling rate to produce a time-stamped range signal. The azimuth and elevation angle of the gimbal were also recorded at the same time to correct for relative changes in position of the optical ranging system reference point with respect to the fixed GPS antenna at the OCTL.

Postprocessing of meteorological data for the experiment duration was then used to calculate the refractive index of air in order to correct for the path difference between the optical and true path [4].

We analyzed the end-to-end signal powers to determine the required laser signal strength and the optimum detector. The return signal strength was estimated from Equation (1). The terms are defined in Table 1. This expression is a modified version of the general expression given in [5]; it reflects the PRBS modulation format, and the reduction of atmosphere beam steering effects on the 2-mrad-wide beam. Because of the "large" retroreflector aperture, the return beam is fully captured in the telescope aperture and the range dependence of the power is there proportional to R^{-2} and not R^{-4} of typical retroreflector experiments.

$$P_d = \varepsilon P_T \eta_{TX} L_P \eta_{atm}^2 \xi \eta_{Rx\_Tel} \left(\frac{D_{retro}}{R\theta} \right)^2 \tag{1}$$

Table 1. Description of terms in Equation (1).

Symbol	Parameter
P_T	Transmitted laser power, W
η_{atm}	Atmospheric transmittance
η_{TX}	Transmission efficiency
θ	Transmitter beam divergence, rad
L_P	Pointing loss, dB
D_{retro}	Retroreflector diameter, m
ε	Retroreflector efficiency
ξ	Truncation loss by telescope secondary
η_{RX_Tel}	Receive telescope transmission

At the 1700-m range, the diameter of the first two dark rings of the retroreflected Airy pattern (8.8 cm and 16 cm) are centered on and are less than the receiving telescope aperture. When projected of the beam from behind the 5-cm secondary, the center of the Airy disk pattern of the retroreflected beam is obscured by the secondary. Table 2 gives an analysis of the link with the estimated values of the propagation losses. The estimated received power at the detector is 2.6 μW; this corresponds well to the measured SNR values of 50 to 100 for our detector.
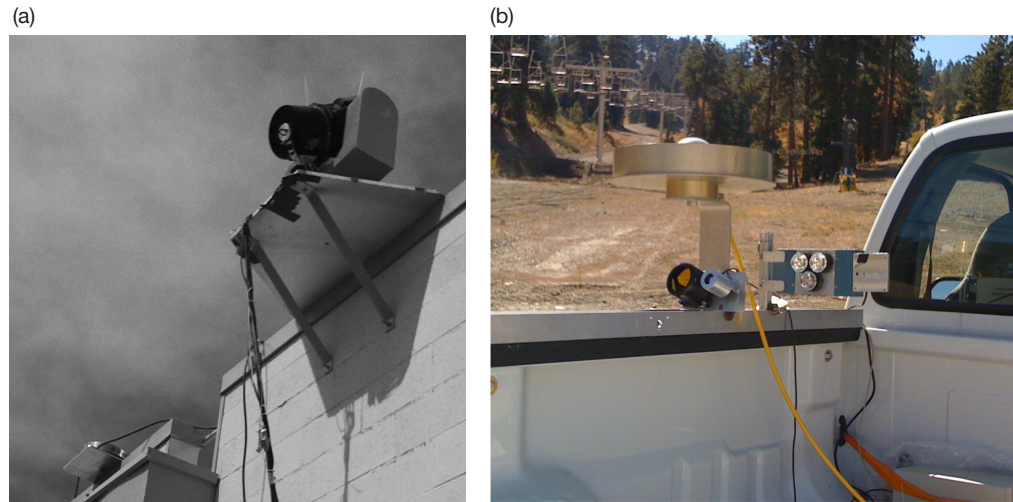
Table 2. Analysis of ALURE horizontal path.

	Value	dB
Transmitted power at output aperture, W	0.4	–4.0
Beam divergence, rad	2.00E–03	—
Range, m	1700	—
Space loss	—	–10.6
Retro diameter, m	0.05	–26.0
Retroreflector efficiency	0.95	–0.2
Fiber coupling efficiency	0.62	–2.1
Transmitter loss	0.9	–0.5
Pointing loss	0.9	–0.5
Atmospheric transmission loss	0.64	–1.9
Receiver transmission	0.5	–3.0
Truncation loss	0.2	–7.0
Power on detector, W	2.6E–06	–55.8

IV. Experiment Setup

Figure 5 shows the experimental setup; (a) is the setup at the OCTL and (b) is the image of the setup on the truck. In (a), the ALURE laser telescope is in the upper right-hand corner looking down on the valley at the truck. In the bottom left corner of (a), the GPS choke ring antenna can be seen at the OCTL.

The ALURE telescope was mounted on a two-axis elevation/azimuth gimbal system. In order to meet the 10-cm error requirement for this test, a precise survey of the ALURE gimbal and telescope, as well as the location of the ALURE center of rotation relative to the GPS receiver, was performed. The OCTL building wall on which the system was mounted was also surveyed and was found to lie along a heading of 228.0 deg east of north. The ALURE

(a)   (b)

Figure 5. (a) OCTL test setup and (b) truck setup.

system reports time in UTC seconds, measured range, and the azimuth and elevation angles of the telescope relative to the 228.0-deg heading. The north point on the GPS antenna was aligned with true north to an accuracy of ±5 deg.

The truck start position was in a valley 170 m below the OCTL on a ski slope approximately 1.2 to 1.5 km to the southwest. An I-beam on the truck bed was used to hold the choke-ring antenna, the retroreflector, the optical beacons, and the optical power meter. The north point of the antenna was aligned with the forward direction of the truck to within ±10 deg. The retroreflector was placed 30 cm directly below the GPS antenna such that the center of reflection of the retroreflector was directly below the center of the antenna. The 50-mm retroreflector had a 40-deg field of view and was installed at a 40-deg inclination relative to the truck to compensate for the slope of the ski run. A power meter placed next to the retroreflector could record the laser power at the retroreflector; however, the high background overwhelmed any signal measurements. Three beacon high-power light-emitting diodes (LEDs) were positioned at the side of the retroreflector to assist in tracking the truck in broad daylight at sunset. A 10-nm full width at half maximum (FWHM) narrowband filter in the ALURE receiver optical train ensured good SNR performance during the daytime while tracking on the 780-nm gallium arsenide (GaAs) LEDs.

GPS data were recorded continuously from both locations. The GPS receiver operating at OCTL was a Trimble NetR5 geodetic receiver. Both a Trimble NetR5 and an Ashtech Micro-Z receiver were installed on the truck and were operated from the same antenna using a splitter. A Paro Scientific Met 3 package measured temperature, pressure, and humidity on the truck, recorded on the Trimble through an RS-422 port. These data were used to calculate both the refractive index along the path and the effects of the troposphere. Power to the electronics was provided from an inverter attached to the truck's battery.

Figure 6 shows the view of the ski run from the ALURE vantage point. During the experiments, the truck speed was increased from 2 to 11 m/s, the maximum speed deemed safe for the terrain. The laser measured the range to the retroreflector and recorded the time, the range to the truck, the elevation, and the azimuth of the gimbal for postprocessing. The truck was stopped for 20 min at the beginning and end of each run to allow stationary GPS tracking at longer GPS arc lengths.

V. Test Results

The test was conducted successfully. The data from the GPS receivers at both locations were collected. The laser successfully provided a range return from the retroreflector. Measurement data from the laser, the GPS receivers, and the metrology data were recorded and postprocessed. The GPS relative positions were calculated using the algorithm described. The metrology data were utilized to estimate the troposphere-related refraction index of the laser. The correction was applied to the laser range and compared kinematically to the GPS relative range. Results show RMS agreement to 4.2 cm.

A major challenge overcome during GPS postprocessing was the significant blockage encountered. The truck test was conducted in the valley in an environment with trees and ski

7.9 deg ← → 11.3 deg

−8.7 deg

−13.8 deg

**Figure 6. Field of view for the ALURE looking down on the truck route.
The truck followed the road to the left of the ski lift.**

lifts, obscuring the line of sight to the GPS satellites, and we experienced varying degrees blockage on each run. On every run, both receivers lost lock on most satellites. While six or seven satellites would be visible at the top and bottom of the run, one point on the run had particularly severe blockage. At this point, the number of tracked satellites would briefly (for 1 to 2 epochs) drop to three — an insufficient number for positioning. Five satellites are required for the short-baseline technique described; six are preferred. In general, the Ashtech tracked more satellites over each run than the Trimble. The results presented are for the Ashtech receiver.

The simple short-baseline technique was able to statistically converge over the short arc lengths due to the carrier-phase-only residuals with position errors annihilated. The ambiguity was resolved and proved to be consistent with the laser ranging results. When the number of satellites tracked was reduced to three, this method did not re-initialize the ambiguity. Instead, the batch processing of the available data for each run enabled the ability to resolve ambiguities on either side of the discontinuity and show consistency across the satellite gap. While it improved continuity over the run for the three satellites tracked, three satellites are still insufficient to provide a relative position estimate. The technique only provided position estimates when at least five satellites were visible.

ALURE measures the optical path length S_{opt} between two points z_1 and z_2; this is given by Equation (2)

$$S_{opt} = \int_{z_1}^{z_2} n(z)\,dz \tag{2}$$

where $n(z)$ is the refractive index at point z. The GPS measures after correction for troposphere effects and multipath contributions measures the distance $R = (z_2 - z_1)$ between

these points. Comparing ALURE and differential GPS measurements requires knowledge of the troposphere contribution and of the refractive index along the path. We calculated the refractive index ($n = 1.00021$) for the path from the meteorological measurements made at the OCTL and at the truck and relations given in [6]. The value used was the average of the values at both locations — an approximation reasonable over such a short altitude variation. With n a constant over the range, $n(z)$ can be taken outside the integral in Equation (2) to yield the range that is determined by $c\Delta\tau n$, where c is the speed of light in vacuum and $\Delta\tau$ is the time of flight of the optical signal.

Results of a typical run are depicted in Figure 7, in which (a) shows the GPS compared with the ALURE range, while (b) shows the difference betwen the two solutions. Outlier errors greater than 0.5 m in the carrier phase have been removed from the data. The outliers and data gaps consistently occurred for 1 or 2 points in any run when the number of satellites dropped below five. The algorithm did not have cycle slip detection or repair implemented. When the truck passed a blocked region, cycle slips may have been introduced, which would cause the algorithm to have an error since the algorithm could not estimate ambiguities where too few satellites were visible. This error naturally fixes itself when more satellites are visible and the algorithm naturally estimates the integer over the longer, healthy arc. The results show that there is a slight dynamic variation consistent with attitude changes of the truck. However, attitude was not measured on the truck and in our calculations we assumed that the retroreflector was always directly below the GPS antenna. The slope of the mountain contributed to the bias observed. We believe that the measured oscillation in the results is real and reflects the motion of the truck on the uneven ski run terrain.
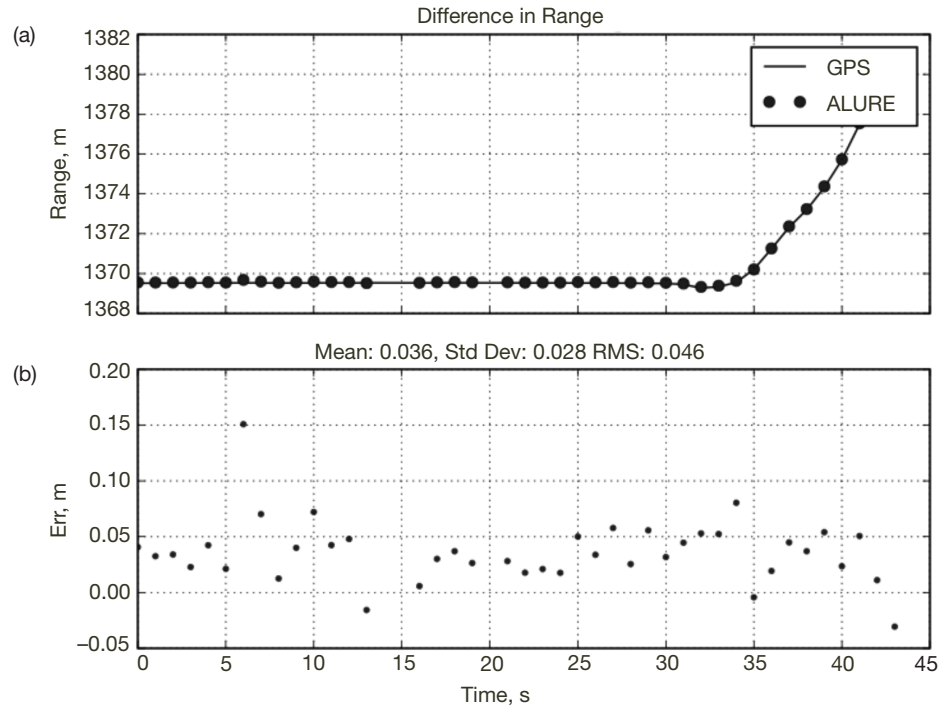

Figure 7. (a) GPS comparison of range with ALURE; (b) difference between the two solutions.

Table 3 provides the comparison of the three solutions over four runs. The errors are in centimeters. All four runs show consistent results and all are under 10 cm RMS error, the target for this experiment.

Table 3. Difference of GPS range results relative to ALURE
for four runs (values in centimeters).

	Run 2	Run 3	Run 4	Run 5
Least Squares Mean	2.2	2.2	4.3	3.6
Std Dev	2.8	2.0	4.2	2.8
RMS	3.6	2.9	6.0	4.6

VI. Conclusions

This article documents the dynamic test of optical laser ranging compared with GPS precise relative position estimation. A laser ranging system was developed that demonstrated ~5-cm accuracy at SNR levels >5 dB. A short-baseline technique was implemented to resolve the wide-lane carrier phase integer ambiguity between the static base station and the dynamic truck. The range to a moving truck was measured simultaneously by both the GPS and laser ranging techniques. Results showed a mean error of less than 4.3 cm and standard deviations less than 4.2 cm. The RMS value differences were less than 6 cm and the average RMS values between the runs was 4.2 cm.

Based on these results, a flight test was planned. The aircraft is to be instrumented with the retroreflector and both Ashtech and Trimble receivers and integrated to the aircraft's GPS antennas. The GPS solution will be compared with the ALURE as before. The challenge will be the correct estimation of troposphere refraction on the laser and on the GPS solution. In the present case, the relative altitude difference was only 500 m. Troposphere errors nearly cancel over these short baselines.

References

[1] J. D. Wolfe, W. R. Williamson, and J. L. Speyer, "Hypothesis Testing for Resolving Integer Ambiguity in GPS," *Journal of the Institute of Navigation*, vol. 50, no. 1, Spring 2003.

[2] W. I. Bertiger, S. Desai, B. J. Haines, N. Harvey, A. W. Moore, S. Owen, and J. P. Weiss, "Single Receiver Phase Ambiguity Resolution With GPS Data," *Journal of Geodesy*, vol. 84, issue 5, pp. 327–337, May 2010.

[3] A. E. Niell, "Global Mapping Functions for the Atmosphere Delay at Radio Wavelengths," *Journal of Geophysical Research*, vol. 101, no. B2, pp. 3227–3246, February 10, 1996.

[4] Edlen Bengt, "The Refractive Index of Air," *Metrologia*, vol. 2, no. 2, p. 12, 1966.

[5] Keith E. Wilson, Joseph Kovalik, A. Biswas, and William T. Roberts, "Development of Laser Beam Transmission Strategies for Future Ground-to-Space Optical Communications," SPIE Symposium on Defense and Security, Orlando, Florida, vol. 6551, April 2007.

[6] V. B. Mendes and E. C. Pavlis, "High-Accuracy Zenith Delay Predictions at Optical Wavelengths," *Geophysical Research Letters*, vol. 31, L14602, 2004. doi:10.1029/2004GL020308